

## **General Disclaimer**

### **One or more of the Following Statements may affect this Document**

- This document has been reproduced from the best copy furnished by the organizational source. It is being released in the interest of making available as much information as possible.
- This document may contain data, which exceeds the sheet parameters. It was furnished in this condition by the organizational source and is the best copy available.
- This document may contain tone-on-tone or color graphs, charts and/or pictures, which have been reproduced in black and white.
- This document is paginated as submitted by the original source.
- Portions of this document are not fully legible due to the historical nature of some of the material. However, it is the best reproduction available from the original submission.

DOE/JPL-956046-82/4  
9950-718

AN EBIC STUDY OF HEM POLYCRYSTALLINE SILICON

May 27, 1982

JPL Contract No. 956046 ✓

by

T. Koch\* and D. Ast

Materials Science and Engineering  
Bard Hall, Cornell University  
Ithaca, New York 14853



The JPL low-cost solar array project is sponsored by the U.S. Department of Energy and forms part of the Solar Photovoltaic Conversion Program to initiate a major effort toward the development of low-cost solar arrays. This work was performed for the Jet Propulsion Laboratory, California Institute of Technology by agreement between NASA and DOE.

\* Permanent address: Hewlett-Packard Company, 1020 North Circle  
Boulevard, Corvallis, Oregon 97330.

(NASA-CR-169296) AN EBIC STUDY OF HEM  
POLYCRYSTALLINE SILICON (Cornell Univ.,  
Ithaca, N. Y.) 20 p HC A03/ME A01 CSCL 10A

N82-32864

G3  
5/44

Unclas  
33546

## ABSTRACT

Low-cost silicon for solar cells grown by the heat exchanger method (HEM) has been studied in the electron beam induced current (EBIC) mode of a scanning electron microscope (SEM). Comparisons were made between the defects observed optically and the recombination centers visible in EBIC. Much of the HEM material was single crystalline, but structural defects were found from areas near the corners of the grown material. Most of these defects consisted of linear twin boundaries and grain boundaries. The electrical activity of these boundaries was dependent on symmetry of the boundaries. Symmetric twin boundaries did not exhibit recombination activity while unsymmetric twin boundaries were electrically active.

## INTRODUCTION

Many new methods of crystal growth have been developed in recent years to provide low-cost silicon for solar cells (1). One of these methods is the heat exchanger method (HEM). In this casting method, a silicon seed crystal is placed in the bottom of a crucible on a heat exchanger. Poly-crystalline material on top of the seed is heated by a graphite resistance furnace in a vacuum of 0.1 torr, and the seed is cooled by forcing helium gas through the heat exchanger (2). A schematic diagram of the furnace is shown in Figure 1. The final material is mainly single crystalline with most of the defects near the upper corners of the block. Defects in the crystal structure affect the performance of the resulting solar cell. Defects may arise during the growth process (i.e. ingrown defects) or may be induced when the solidified material cools and thermal stresses are relieved by plastic deformation (dislocation movement at high temperatures, twinning at lower temperatures). Differentiation between grown-in and deformation induced defects is usually difficult but very useful for improvements in the growth process.

Most of the material examined contained few defects. The large majority of the crystal defects that were found were located in areas near the edges of the block where large thermal gradients and stress concentrations exist during growth and cooling. Localized defects such as grain boundaries, incoherent twins, and partial dislocations at coherent twins can affect the electrical properties of the semiconductor by providing recombination centers for minority carriers (3,4). The

resulting drop in the minority carrier diffusion length reduces the solar-cell efficiency. The main crystal defects observed in this HEM material were grain boundaries, coherent and incoherent twin boundaries. These defects were studied both optically, after an etch process, and in the EBIC mode (Electron Beam Induced Current) of a SEM (Scanning Electron Microscope). By direct correlation, defects observed in the optical microscope were examined in EBIC for electrical activity. Good reviews of the EBIC technique are given in References 5 and 6.

#### EXPERIMENTAL METHOD

The HEM material was received in a block with dimensions of 9in x 3in x 3/8in. The crystal growth axis was along the 3in. direction. Several strips 2mm in width were sliced from the block at a 60 degree angle to the growth direction, from an area containing many different grains. The strips were cut into 1 cm x 1 cm x 2mm pieces, and ground to a thickness of 0.5mm by sanding with silica carbide paper followed by polishing with a syton solution to obtain a mirror finish.

Samples for optical microscopy were etched in a solution of  $\text{HNO}_3\text{:HF:HAc}$ , 5:1:1, to delineate the boundaries.

The EBIC technique requires a p-n junction or a Schottky barrier to collect the carriers produced by the electron beam. A Schottky barrier

was used in this study. A schematic diagram of the experimental set-up for EBIC is shown in Figure 3.

Schottky diodes can be produced reproducibly only on smooth and extremely clean surfaces. The RCA cleaning procedure was found to give the most consistent results. The samples were initially cleaned in separate solutions of trichloroethylene, acetone, and methanol using an ultrasonic cleaner, then heated in a mixture of unstabilized 30% hydrogen peroxide, ammonium hydroxide, and deionized water. These two steps removed any organic material present on the silicon surface. An ionic cleaning was also performed with a mixture of unstabilized 30% hydrogen peroxide, hydrochloric acid, and deionized water. The samples were dipped in a 3:1 solution of deionized water and hydrofluoric acid to remove the  $\text{SiO}_2$  surface layer and promptly placed in a vacuum system of  $10^{-6}$  torr to prevent oxide regrowth on the surface. A thin film of Al (500Å) was deposited onto the silicon through a grid to produce 3 x 2mm diodes. The samples were mounted on Al disc with a carbon-based, low-resistance, contact cement to provide an ohmic back contact to the Schottky diodes.

## RESULTS

Most of the specimens consisted of large size grains and areas of parallel striations, which were generally attributed to the presence of twin boundaries (Figure 3). Note that in Figure 3 the etch rate for

defects is very different for the parent crystal (or Matrix) and the twin bands. This can be seen by following the scratch marks which are--although clearly continuous across the twinned region--hardly etched in the latter. Similarly, the density of visible dislocation etch pits is much greater in the darker matrix areas as shown in the micrograph of Figure 4. Assuming the twins are coherent first order twins--since the boundaries were not electrically active in EBIC--and noting that the angle between the twins visible in Figure 3 is  $120^\circ$ , the parent crystal must be approximately  $\{111\}$  (Figure 5) and the twinned regions have approximately a  $\{115\}$  orientation. The surface orientation of approximately  $\{111\}$  was confirmed by x-ray diffraction using a real time Laue x-ray reflection camera. Note that the etchant described above is highly anisotropic since the deviation from the  $\{111\}$  orientation caused large differences in the etching of defects in the matrix and the twin sections.

Since the resolution of the optical microscope is similar to that of the SEM in the EBIC mode, defects observed in the optical microscope can easily be compared to the electrical activity of defects in EBIC. Because of the scan sequence the EBIC pictures are left-right reversed and rotated by  $90^\circ$  when compared to optical micrographs. This should be kept in mind when comparing figures.

The correlation between the defects found in optical microscopy and the recombination effects of the defects in EBIC microscopy was usually good. A low magnification EBIC micrograph of the same area as in Figure 3 is shown in Figure 6a. The twin structure is easily identified

because of contrast difference between the twin bands and the parent crystal. Close inspection of the micrographs, Figure 6c, reveals that there is no electrical activity (dark lines in EBIC) associated with the twin boundaries, as opposed to the grain boundary in the upper left-hand corner of the higher magnification EBIC micrograph in Figure 7. Coherent  $\{111\}/\{111\}$  twin boundaries with little or no EBIC contrast have been reported elsewhere (7,8).

The twin bands in Figure 3,6,7, and 9 raise the question of how and when these bands grew and/or came together. Most likely the twin bands were deformation induced after solidification. Models of the twins as arrays of twinning dislocations shows that attractive stress field existed between two closely spaced twin bands (e.g. Fig. 9c). It appears that twins of equal thickness can join without producing a detectable boundary either by etching (because of the low sensitivity of the anisotropic etch) or by EBIC (because of the absence of strong recombination centers). In joined twin bands, see Figure 5, the expected boundary is a symmetric  $\{221\}/\{221\}$  second order twin. In the atomic model of this boundary by J. A. Kohn, no dangling bonds are present if a zig-zag mechanism is used for the discontinuity surface (9). Since electrical activity of defects is usually associated with broken bonds, the low EBIC activity is compatible with Kohn's structural model. Work is now being conducted to improve the Schottky barriers, to achieve higher EBIC resolution and to carry out temperature dependent EBIC in order to obtain a better understanding of the electrical activity of these higher order twins.

When symmetry was not preserved at the intersection of the twin bands, strong recombination was observed in EBIC. High magnification optical and EBIC micrographs of some of the twin bands which did display electrical activity at the intersection are shown in Figures 8 and 9. Figures 8a and 8b are optical micrographs of the same areas imaged in the EBIC micrograph in Figure 8c. The small nonuniform top corner seen in Figure 8a, which by definition must be a incoherent first order twin boundary, was seen in the EBIC micrograph as electrically active. Similarly, the asymmetric intersection of the twin bands of unequal thickness shown in Figure 8b with an area of incoherent first order twin boundaries resulted in strong recombination in EBIC as seen in Figure 8c. However, recombination centers were not limited to areas of incoherent first order twin boundaries. An intersection of twin bands of slightly unequal thickness with no visible etch lines was found to be electrically active in EBIC (Figures 9a and 9b). One may speculate that since this twin intersection was not quite symmetric, a "non-restorable" (see ref. 9 for more discussion) second order twin boundary was formed. Due to the anisotropic etchant, the boundary was not etched and is therefore not visible in the optical micrographs.

The twin bands of Figure 9c did not join, but instead formed some first order twins. The trace of the ending of the twin on the left side of Figure 9c is compatible with a  $\{112\}/\{112\}$  first order twin, and it was found that recombination in EBIC was limited only to the corners of the twin band (Figure 9d). To the knowledge of the authors, the electrical inactivity of the symmetric first order  $\{112\} \{112\}$  twin has not been reported before. The twin on the right hand side of Fig. 9c is

terminated by 5 sections. The traces are, in the order from top to bottom, compatible with  $\{010\}/\{221\}$ ;  $\{112\}/\{112\}$ ;  $\{112\}/\{112\}$ ;  $\{111\}/\{115\}$  and  $\{100\}/\{211\}$ ; i.e. with the 4 first order incoherent boundaries discussed by Kohn. Only the last segment (#5) is unambiguously electrically active. Section 3 and 4 appear to be active but are too short to be identified in EBIC. Fig. 9e is another demonstration that  $\{112\}/\{112\}$  first order twins are electrically inactive. In general electrical activity was associated with non-symmetric boundaries; i.e., recombination effects were not observed for coherent  $\{111\}$  twins or for twins whose traces were compatible with  $\{112\}/\{112\}$  first order twins or with symmetric  $\{221\}/\{221\}$  second order twins.

Recent work by B. Cunningham et al. determined that  $\{115\}/\{111\}$  second order twin boundaries are electrically active in edge defined film growth silicon (10). The same twin boundary was also found to exist in HEM silicon with the only notable difference that the twin thickness was about 1 micron instead of 0.1 micron as for EFG silicon which is expected since the cooling period for HEM silicon is considerably longer than for EFG silicon resulting in different equilibrium defect structure. An optical and SEM micrograph of an etched specimen exhibiting the boundaries are shown in Figure 10. A schematic of the boundaries is shown in Figure 11. The linear twin bundles are alternating sections of coherent first order twins and incoherent second order twins of the  $\{115\}/\{111\}$  type. Figures 12a and 12b are EBIC micrographs of the alternating  $\{115\}/\{111\}$  first and second order twin boundaries. The dark dots represent areas of strong

recombination at the  $\{115\}/\{111\}$  second order twin boundary in agreement with the findings of Cunningham et al.

Figure 13a shows an EBIC micrograph of a highly twinned region in HEM solar cell silicon. Many of the twin traces, for example those marked A,B,X,Y and Z, are not electrically active and are only visible because the crystals separated by the boundaries are at different orientations to the  $\langle 110 \rangle$  channels and hence have different EBIC contrast. However, some of the traces are highly electrically active, operating as efficient recombination centers and hence are unaged in the EBIC mode as thick black lines (e.g., traces C, D and E). By measuring the angles between the traces and relating them to the crystallography of twinning it has been possible to determine the plane and order of many of the twin boundaries.

The angle between the traces of the inactive twin boundaries X and Y is  $88^\circ \pm 1^\circ$  and the angle between Y and Z (also inactive) is  $108^\circ$ . These measurements can be explained in the following way: the surface normal of the region marked M is near  $[001]$ ; the traces X and Y are in the directions  $[110]_M$  and  $[1\bar{1}0]_M$  as shown and correspond to first order coherent twins ( $\{111\}/\{111\}$ ) which are known to be electrically inactive; trace Z is in the  $[120]$  direction which makes an angle of  $108.44^\circ$  with  $[1\bar{1}0]_M$  and corresponds to a first order  $\{112\}/\{112\}$  twin (sometimes known as a lateral first order twin), which is, as discussed before, also electrically inactive.

We can assume without loss of generality that the twinning operation from crystal M to  $T_1$  is a  $60^\circ$  rotation about  $[111]$  for which

the transformation matrix is  $\begin{pmatrix} 2 & -1 & 2 \\ 2 & 2 & -1 \\ -1 & 2 & 2 \end{pmatrix}$ . Hence the surface normal of crystal  $T_1$  is  $(2\bar{1}2)$ . Trace A is not electrically active and so the boundary is likely to be a first order twin. The angle between traces A and Y is  $54^\circ$  and  $\bar{Y}$  is  $[10\bar{1}]_{T_1}$ . Looking at the  $(2\bar{1}2)$  plane we find that  $[1\bar{4}3]$  makes an angle of  $56.3^\circ$  with  $[10\bar{1}]$  and since  $[1\bar{4}3]$  lies in the plane  $(11\bar{1})$  the evidence suggests strongly that boundary A is a first order coherent twin on the  $(11\bar{1})$  plane. Trace B is parallel to trace Y and is also a first order coherent twin and, since A and B are nonparallel, the regions marked  $T_2$  and  $T_3$  are related by a second order twinning operation.

According to Kohn (1958) there are three low energy second order twin boundaries -  $\{221\}_1 // \{221\}_2$ ,  $\{115\}_1 // \{111\}_2$  and  $\{114\}_1 // \{114\}_2$ . In all three cases the second order boundary plane is in the same zone as the two first order coherent boundaries, i.e., the  $\langle 110 \rangle$  direction common to both  $\{111\}$  twinning planes. In addition the trace of these second order planes bisects either the acute angle between the first order traces ( $\{114\} // \{114\}$ ), or the obtuse angle ( $\{221\} // \{221\}$ ) or else lies parallel to one of the first order traces  $\{111\} // \{115\}$ . This is true irrespective of the orientation of the specimen surface, and clearly trace C does not correspond to any of these cases. Figure 14 is a higher magnification image of trace C and shows that the trace is faceted, implying that the boundary plane is adopting low energy configurations where possible. The long facet, marked F in figure 2, is  $72.5^\circ$  from trace A,  $19^\circ$  from trace B and  $89^\circ$  from trace Z. It was determined above that A is the trace of a  $(11\bar{1})_{T_1} // (11\bar{1})_{T_2}$  boundary for which the transformation matrix is  $\begin{pmatrix} 2 & 2 & 1 \\ -1 & 2 & -2 \\ -2 & 1 & 2 \end{pmatrix}_{T_1}^{T_2}$ . From this we determine

that the surface normal to crystal  $T_2$  is  $[4\bar{8}1]$  and that trace A is in the direction  $[3\bar{1}4]$  in  $T_2$ . In the plane  $(4\bar{8}1)$ , the vector  $[7.5.\bar{1}2]$  makes an angle of  $73^\circ$  with  $[3\bar{1}4]_{T_2}$  and lies in the plane  $(111)_{T_2}$ . Of course trace analysis on one surface cannot determine the plane of an interface but it is consistent with the available data that the highly electrically active twin boundary C is parallel to  $(111)$  in crystal  $T_2$ . It is likely that the crystal marked  $T_3$  is in the same orientation as M since the twin traces B and Y are parallel. This implies that C is in the  $\sim[2\bar{1}0]_{M/T_3}$  direction (perpendicular to the trace Z). Using the transformation matrices already given we calculate that  $(111)_{T_2}$  is parallel to  $(7.13.5)_{T_3}$ . This is a second order twin boundary that has not been observed before and some TEM work will be necessary to confirm whether this self-consistent analysis is correct.

## CONCLUSION

Solar cell MEM silicon has been investigated using etching and optical microscopy to reveal grain and twin boundaries. EBIC images were compared to those visible in etched specimens. Coherent twin boundaries did not exhibit recombination activity while unsymmetric incoherent twin boundaries and grain boundaries were usually strongly electrically active. However - and this appears to be a new finding - unsymmetric boundaries ( $\{112\}/\{112\}$  first order twin boundaries and  $\{221\}/\{221\}$  second order twin boundaries) did not act as strong recombination centers. Alternating section of coherent first order twins and incoherent second order twins

of the  $\{111\}/\{115\}$  type showed recombination only on  $\{111\}/\{115\}$  incoherent second order twins as noted by previous investigations. The twin defects were most likely deformation induced after solidification and, therefore, improvements in the structure may be possible by varying cooling conditions. A more comprehensive analysis of the defect structures in HEM silicon by transmission electron microscopy (TEM) is required before a complete understanding of the nature of the defects can be obtained.

ORIGINAL PAGE IS  
OF POOR QUALITY

REFERENCES

1. P. D. Maycock, "Overview-Cost Goals in the LSA Project", 14th IEEE Photovoltaic Specialists Conf. Record (IEEE, New York, 1980) 6.
2. F. Schmid and C. P. Khattak, Heat Exchanger Ingot Casting/Slicing Process, Final Report-Phase 1, ERDA/JPL 954373-77/4.
3. T. Doud and K. M. Koliward, "Effect of Grain Boundaries in Silicon on Minority-Carrier Diffusion Length and Solar-Cell Efficiency", Appl. Phys. Lett. 33. (1978) 1009.
4. H. Strunk, B. Cunningham, and D. Ast, "Defect Structure of EFG Silicon Ribbon", Technical Report #6 DOE/JPL Contract No. 954852 (1980).
5. H. J. Leamy, L. C. Kimerling, and S. D. Ferris, "Electron Beam Induced Current", Scanning Electron Microscopy/1978/Vol. I, p. 717.
6. J. I. Hanoka and R. O. Bell, "Electron-Beam-Induced Currents in Semiconductors", Ann. Rev. Mater. Sci., 11. (1980) 353.
7. C. Rao, H. Bates, K. Ravi, 1976 J. Appl. Phys. 47.
8. G. Schwuttke, 1977. Phys. Status Solidi 43.
9. J. A. Kohn, Am. Mineral., 43 263 (1958).
10. B. Cunningham, H. Strunk, and D. G. Ast, "First and Second Order Twin Boundaries in Edge Defined Film Growth Silicon Ribbon", Appl. Phys. Lett., 40(3), (1982), 237.

## FIGURE CAPTIONS

- Figure 1. Schematic diagram of the Heat Exchanger Method technique.
- Figure 2. Schematic diagram of the EBIC process. Electron-hole pairs are generated within the shaded p-type region. Electrons diffuse to the junction where they are collected and then form the beam-induced current.
- Figure 3. An optical micrograph of a twin band structure. Note intersecting twins and differential etching.
- Figure 4. An optical micrograph of twin region showing higher density of etch pits in parent crystal region opposed to twin band region.
- Figure 5. Schematic drawing of twin bands joining.
- Figure 6. EBIC micrographs of twin regions seen in Figure 3 (a, b, c). SEM micrograph in (d) of same area as in (c).
- Figure 7. Higher magnification EBIC micrograph of area in Figure 6(a).
- Figure 8. Optical micrographs in (a) and (b) of joining twins. EBIC micrograph of both areas in (c).
- Figure 9. (a, c, e) are optical micrographs of areas imaged in EBIC micrographs of (b, d, f).
- Figure 10. (a) Optical micrograph of etch region showing parallel twins that stop on a common boundary. (b) High magnification SEM micrograph of twins ending at boundary.
- Figure 11. Schematic sketch of the arrangement of twin boundaries shown in Figure 10.
- Figure 12. (a) EBIC micrograph of twin region seen in Figure 10. (b) High magnification EBIC micrograph showing dotted characteristic of  $(115)/(111)$  first and second order twin boundaries.
- Figure 13. EBIC micrographs exhibiting mainly twin structures.
- Figure 14. High magnification EBIC micrograph of area in Figure 13(a).

ORIGINAL PAGE 19  
OF POOR QUALITY

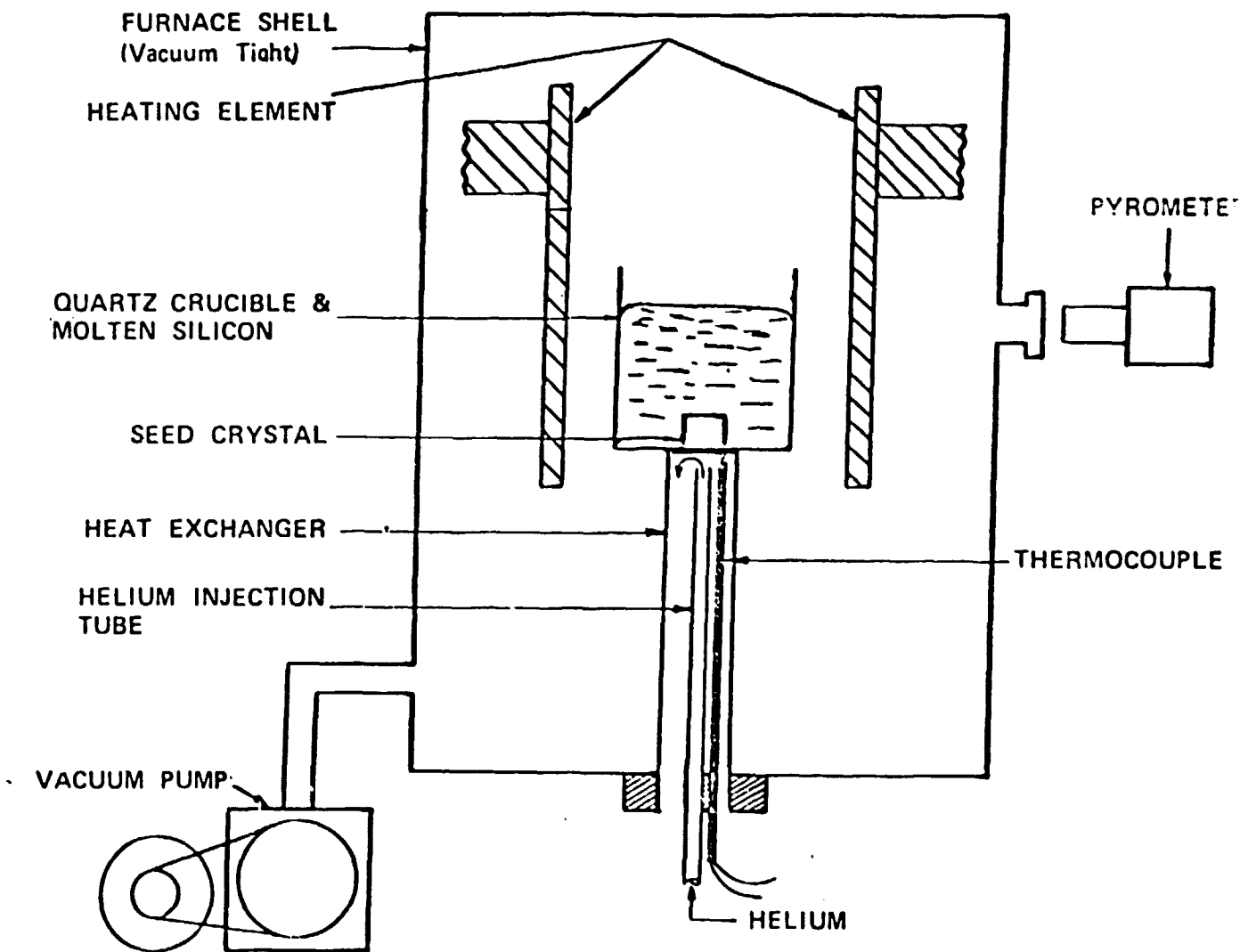


Figure 1. Schematic diagram of the Heat Exchanger Method technique.

ORIGINAL PAGE IS  
OF POOR QUALITY

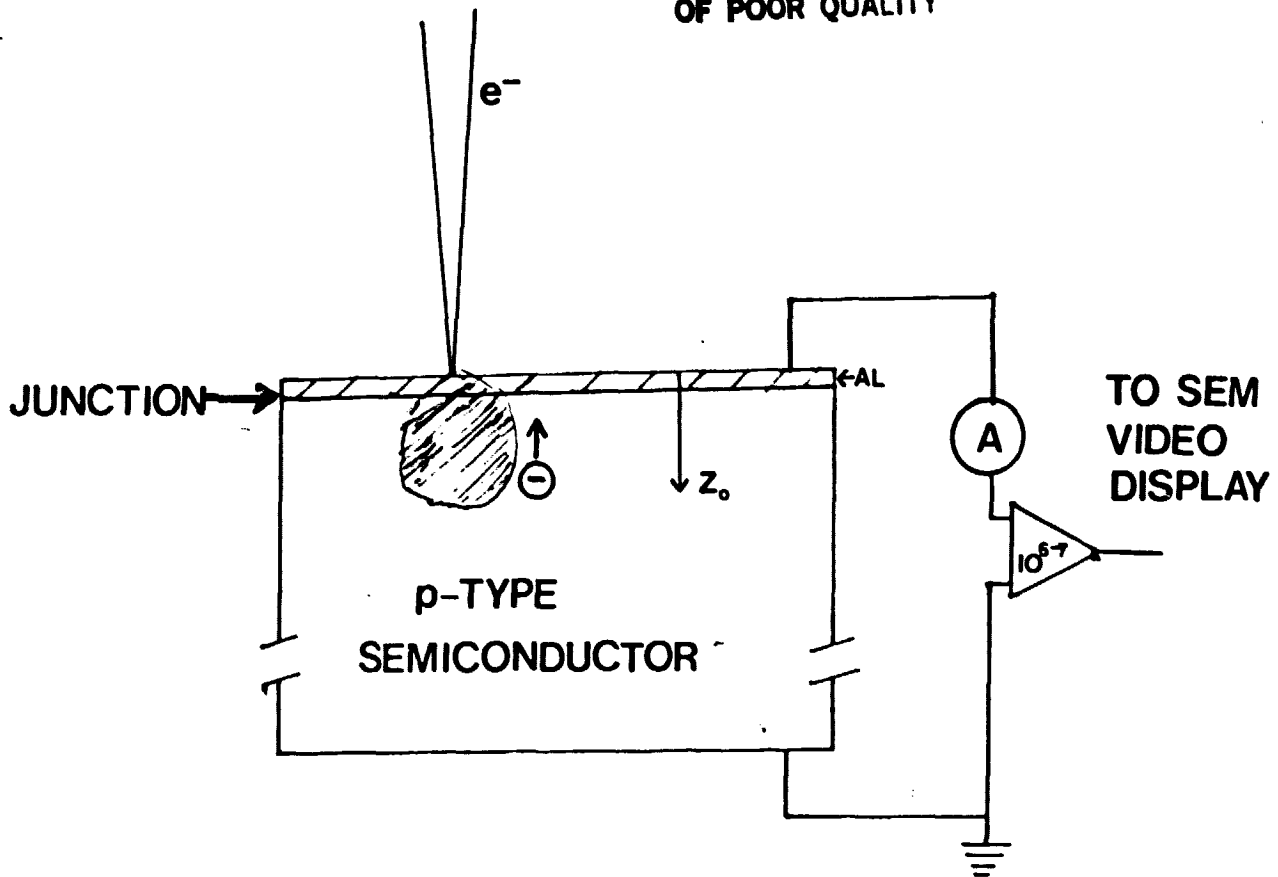


Figure 2. Schematic diagram of the EBIC process. Electron-hole pairs are generated within the shaded p-type region. Electrons diffuse to the junction where they are collected and then form the beam-induced current.

ORIGINAL PAGE IS  
OF POOR QUALITY



Figure 3

ORIGINAL PAGE IS  
OF POOR QUALITY

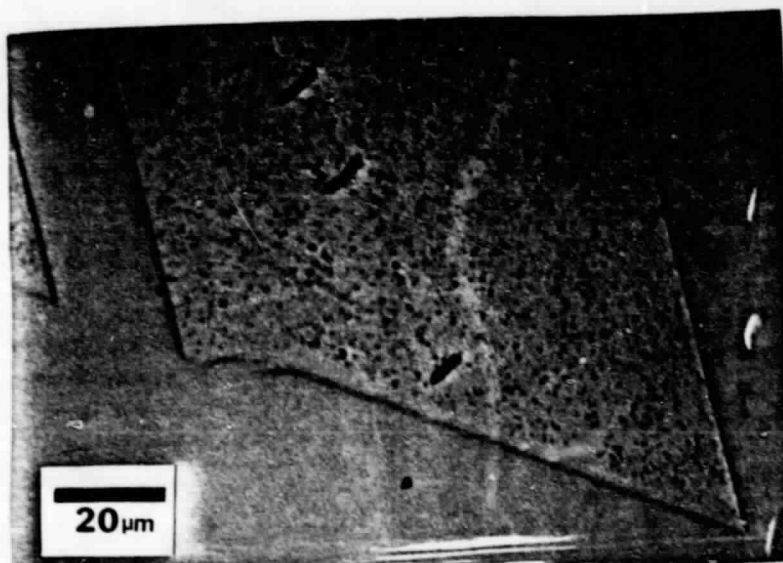


Figure 4

ORIGINAL PAGE IS  
OF POOR QUALITY

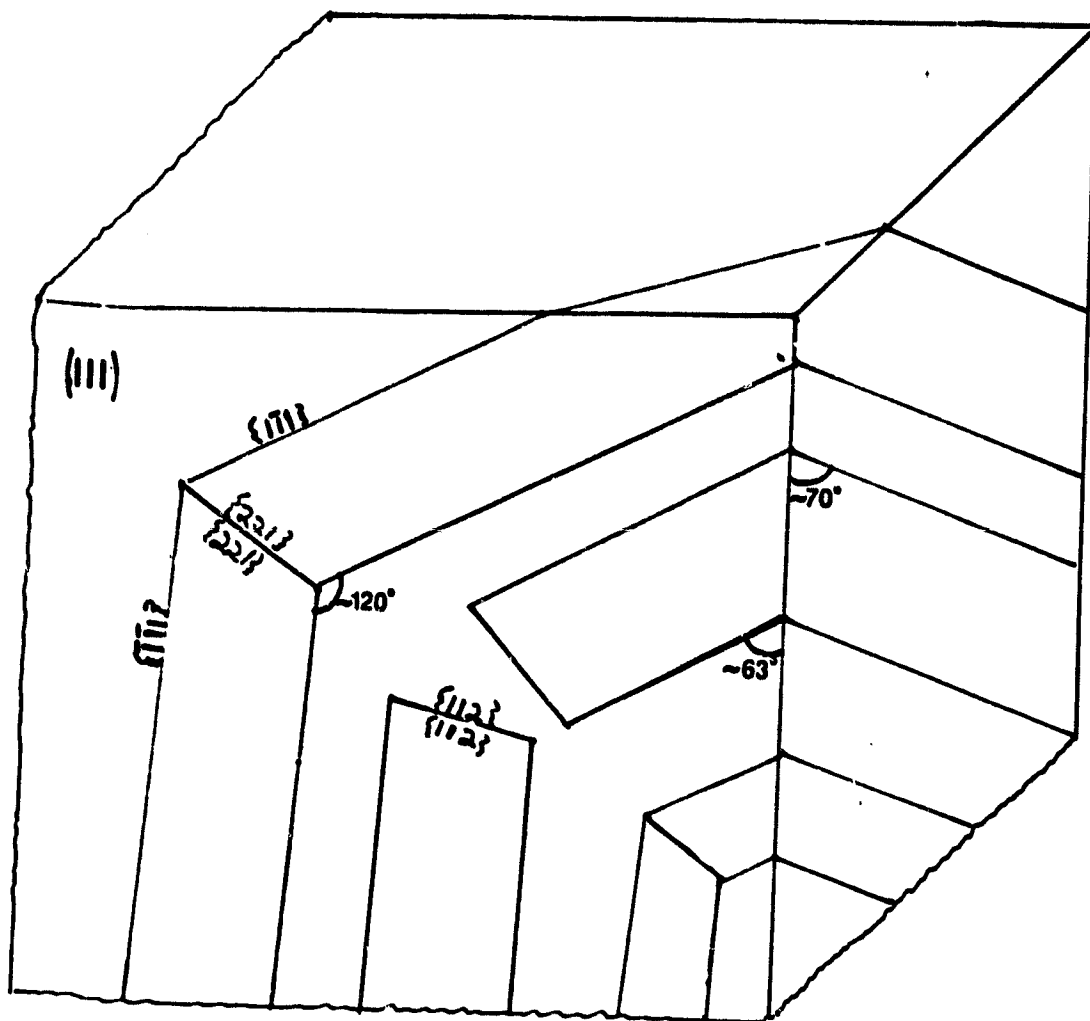
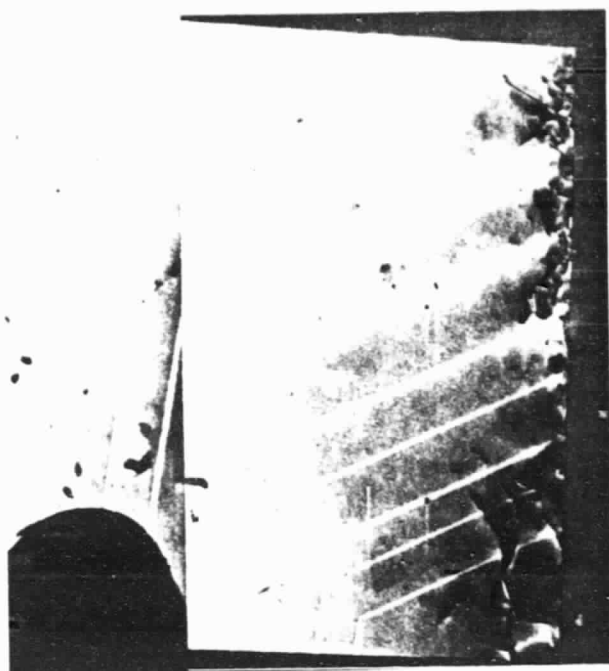
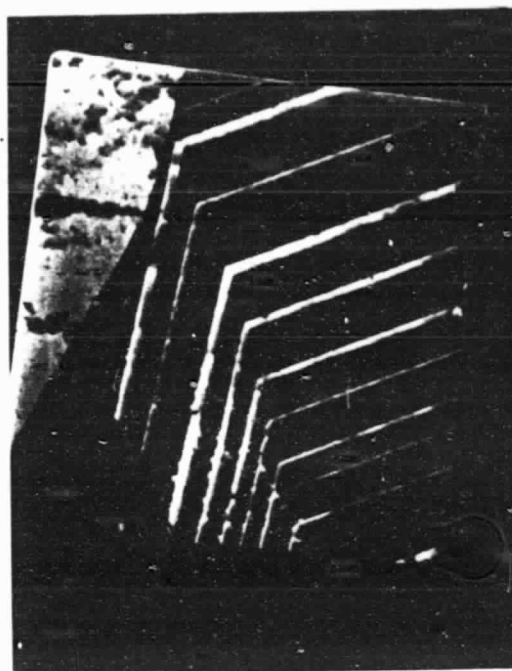


Figure 5

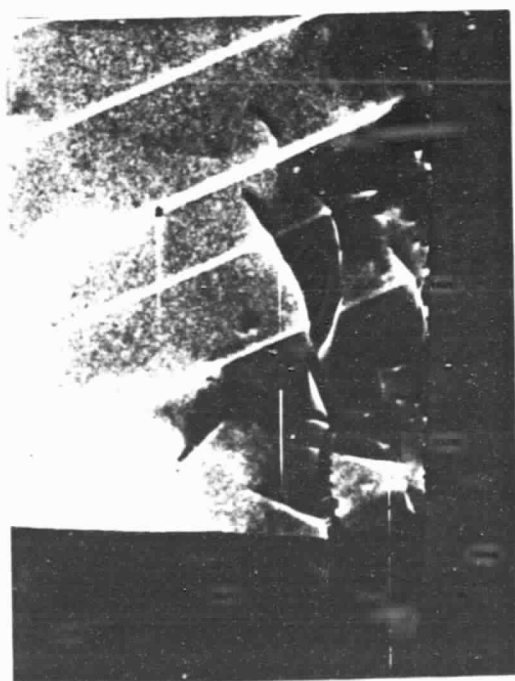


1mm  
(a)

EBIC



1mm  
(b)



100μm  
(c)

EBIC



100μm  
(d)

SEM

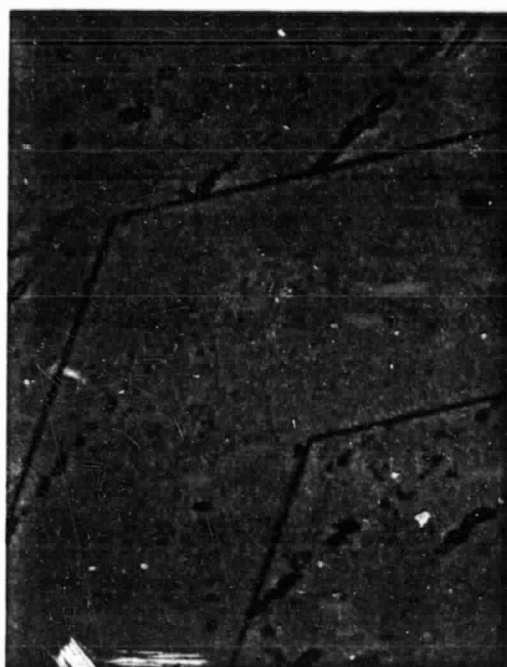
ORIGINAL PAGE  
BLACK AND WHITE PHOTOGRAPH

Figure 6

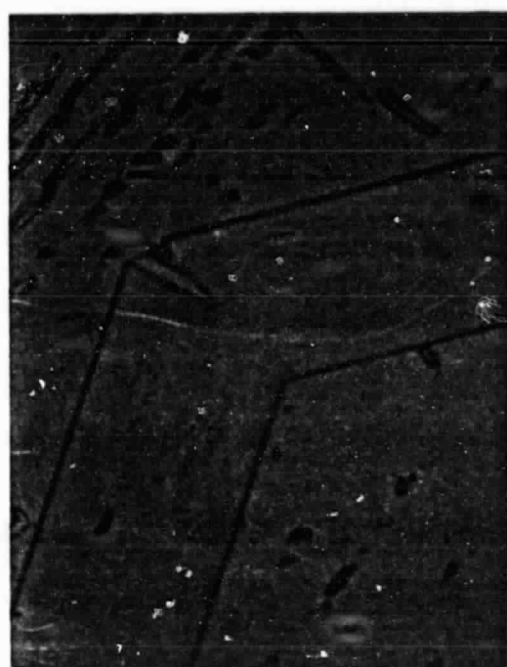


ORIGINAL PAGE  
BLACK AND WHITE PHOTOGRAPH

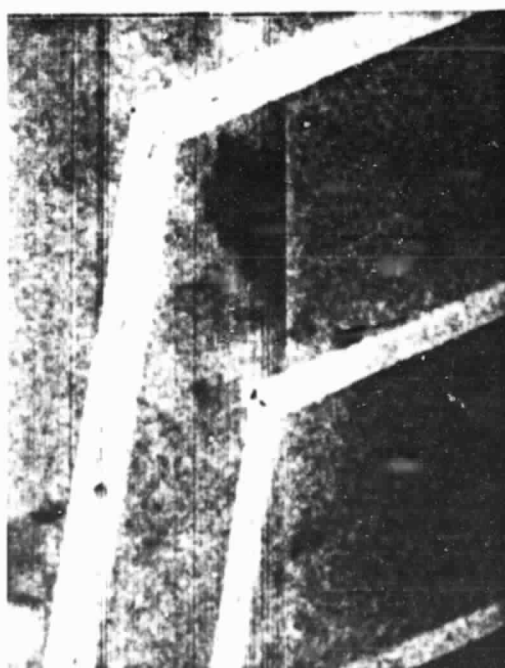
Figure 7



20  $\mu$ m  
(a)



20  $\mu$ m  
(b)

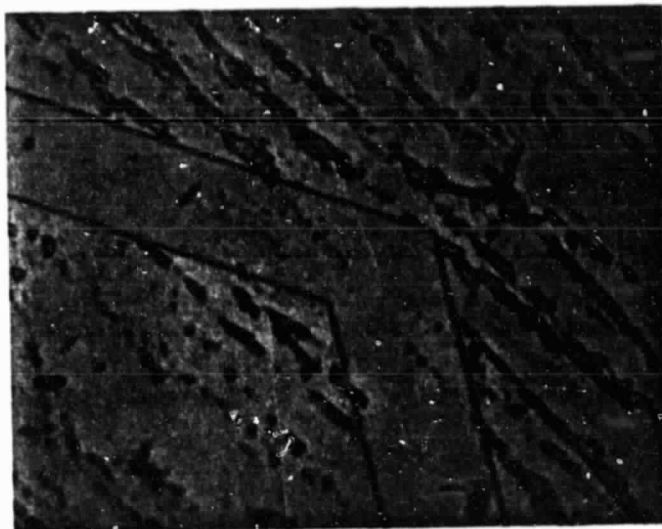


100  $\mu$ m  
(c)

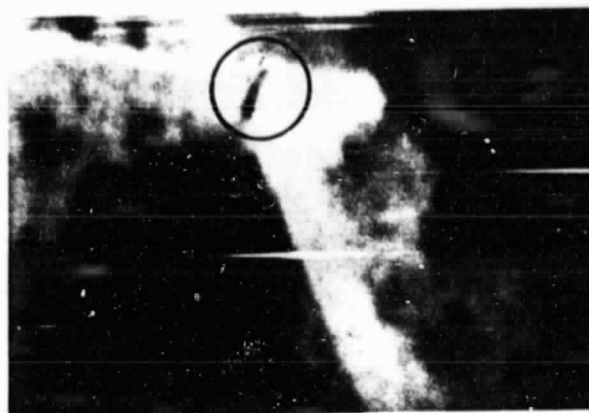
EBIC

Figure 8

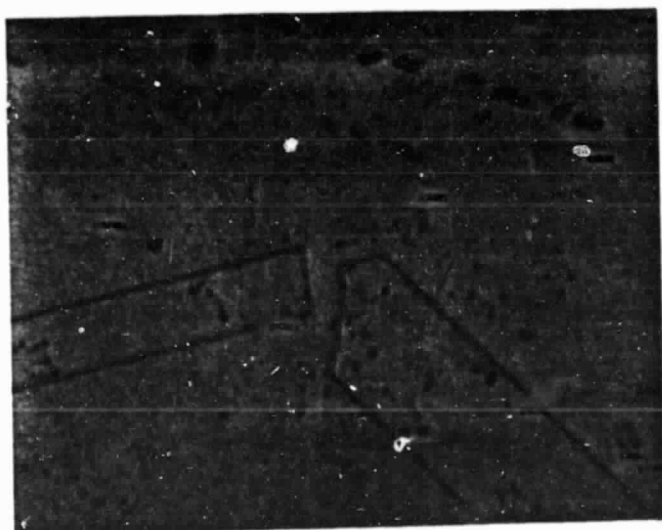
ORIGINAL PAGE  
BLACK AND WHITE PHOTOGRAPH



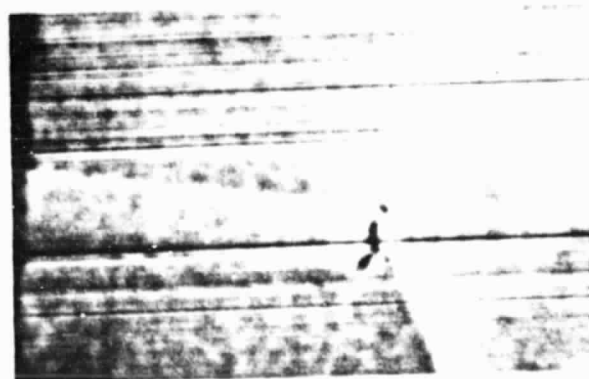
(a)



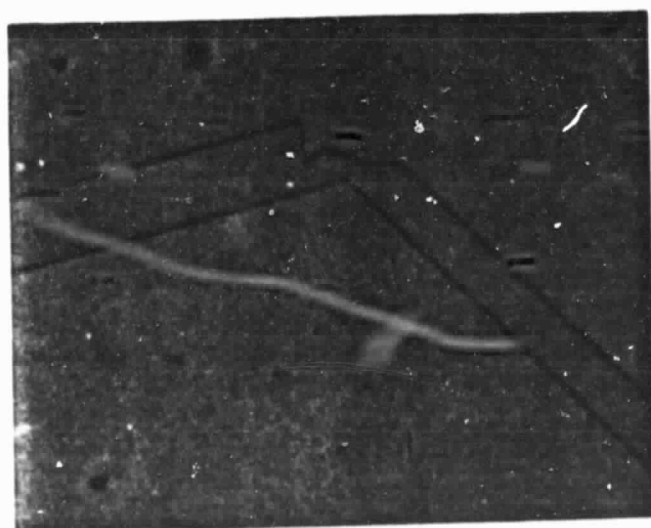
(b)



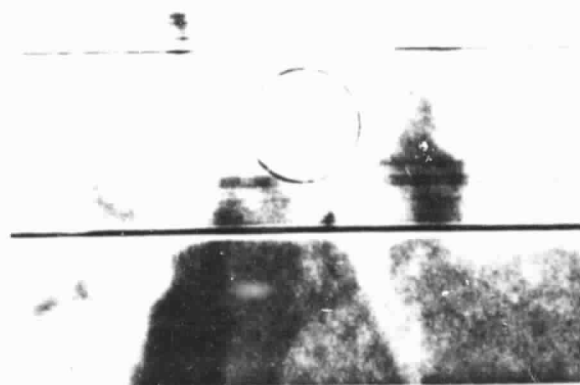
(c)



(d)



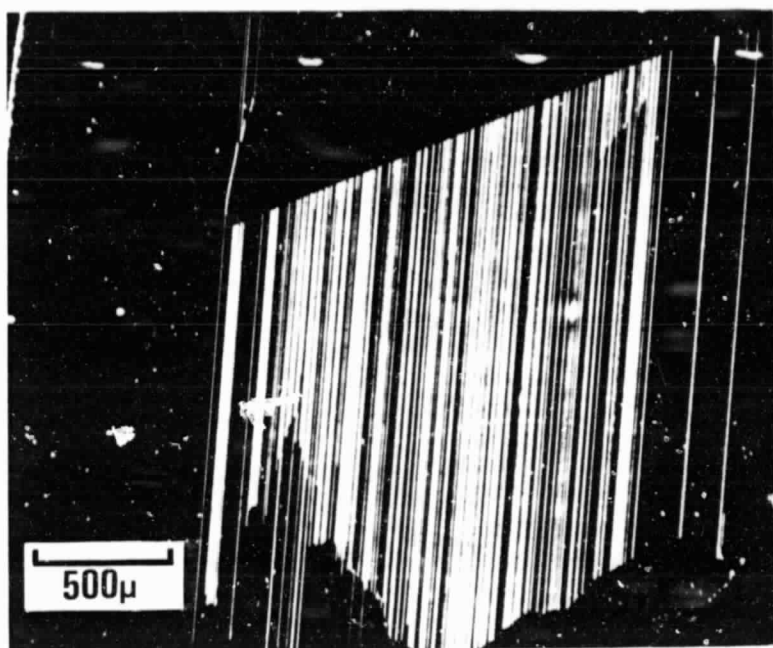
20  $\mu$ m  
(e)



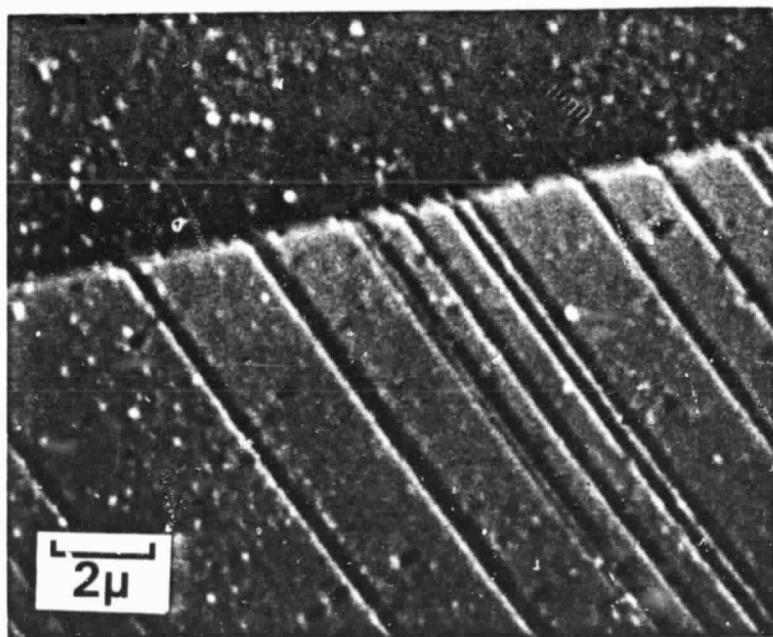
50  $\mu$ m  
(f)

Figure 9

ORIGINAL PAGE  
BLACK AND WHITE PHOTOGRAPH



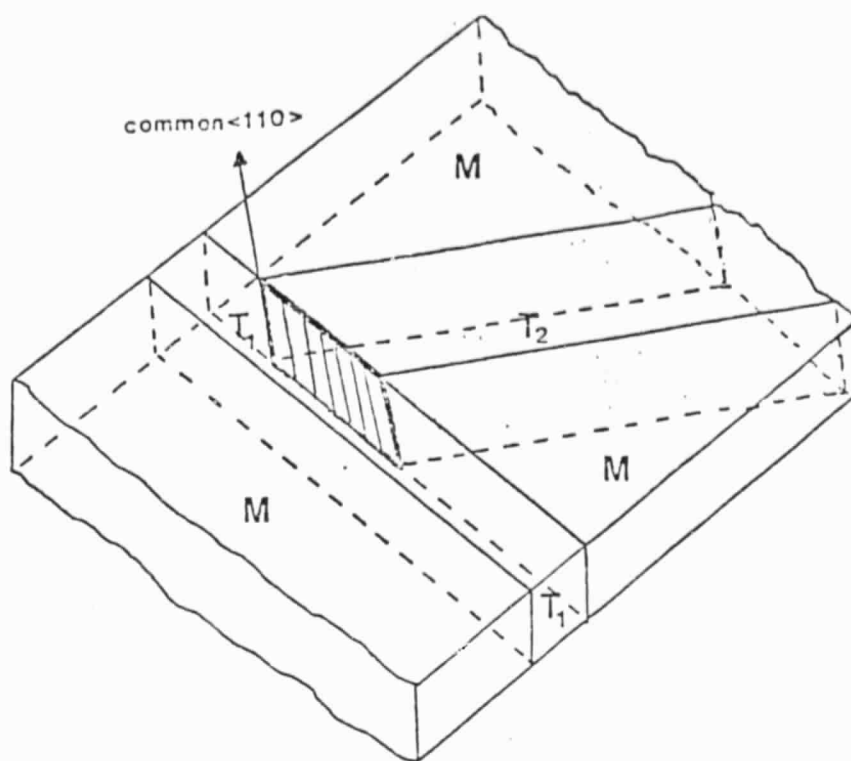
(a)



(b)

Figure 10

ORIGINAL PAGE  
BLACK AND WHITE PHOTOGRAPH



ORIGINAL PAGE IS  
OF POOR QUALITY

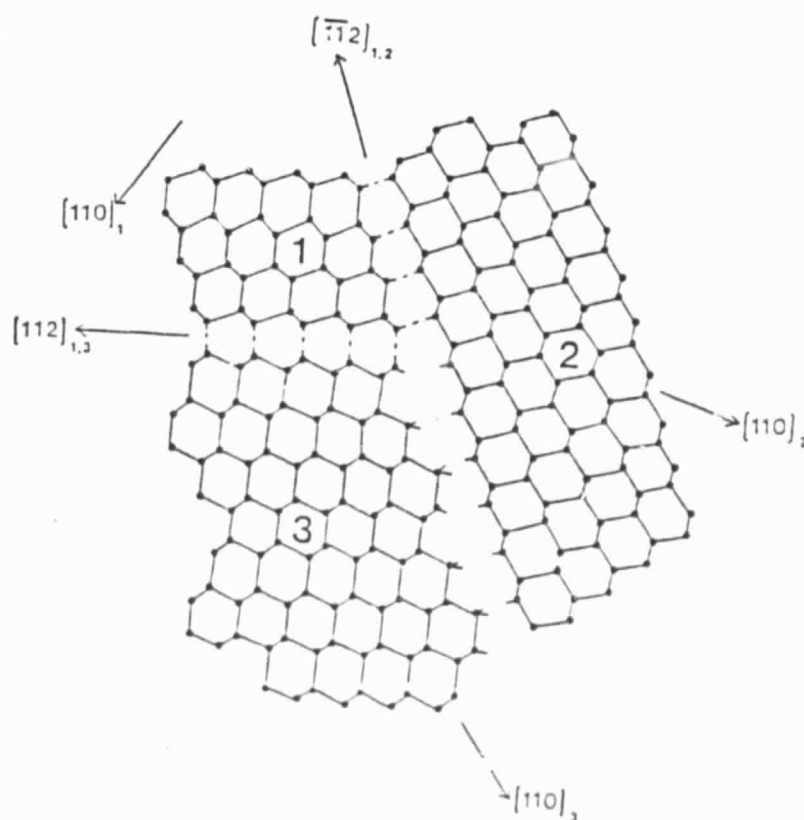
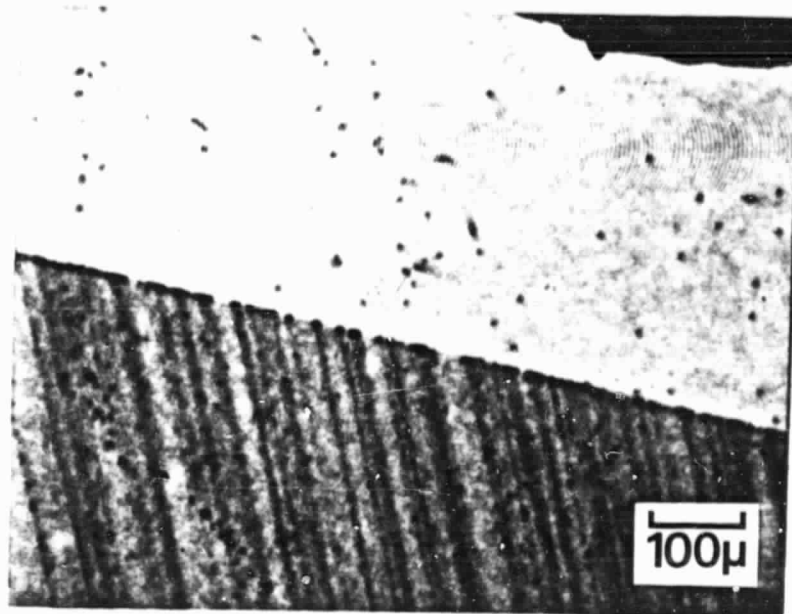
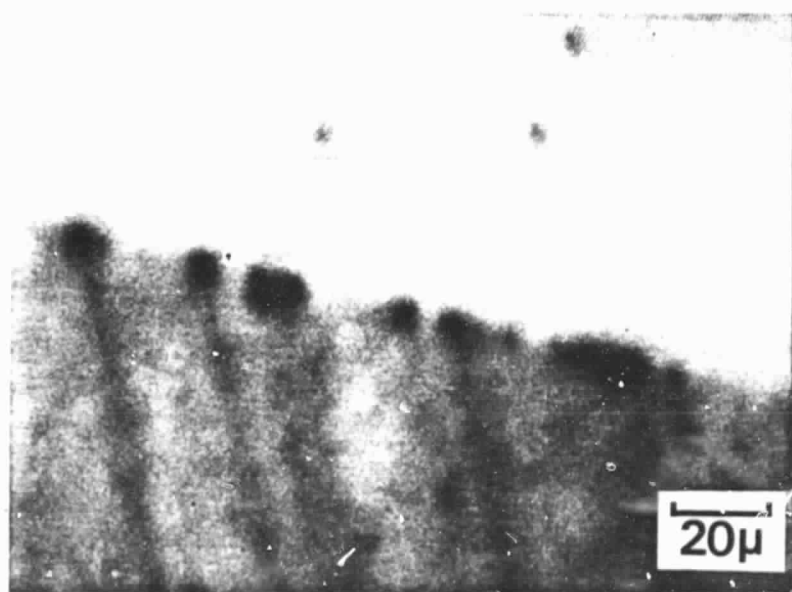


Figure 11



(a)



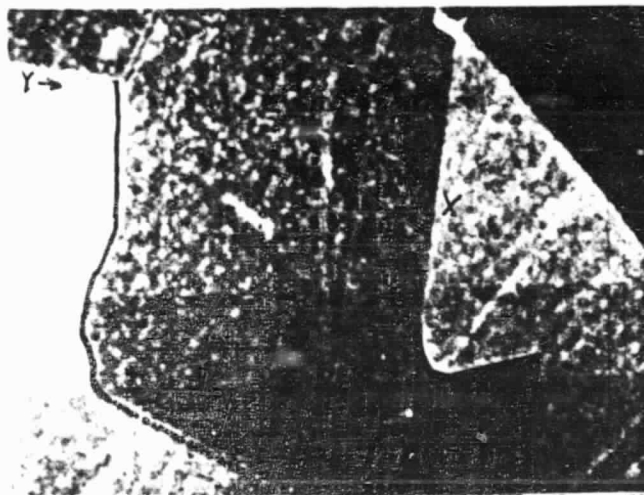
(b)

Figure 12

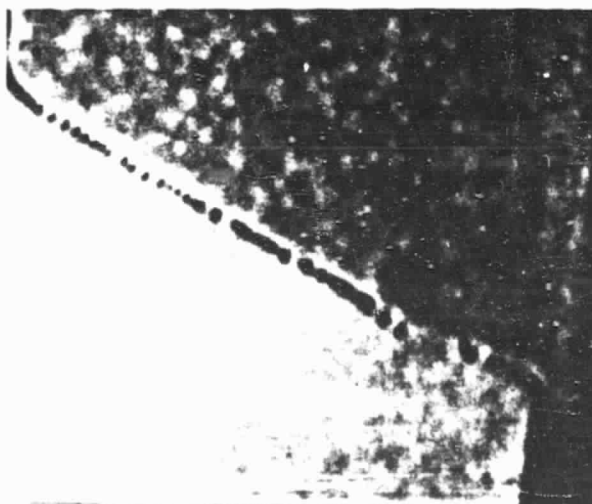
ORIGINAL PAGE  
BLACK AND WHITE PHOTOGRAPH



1mm  
(a)



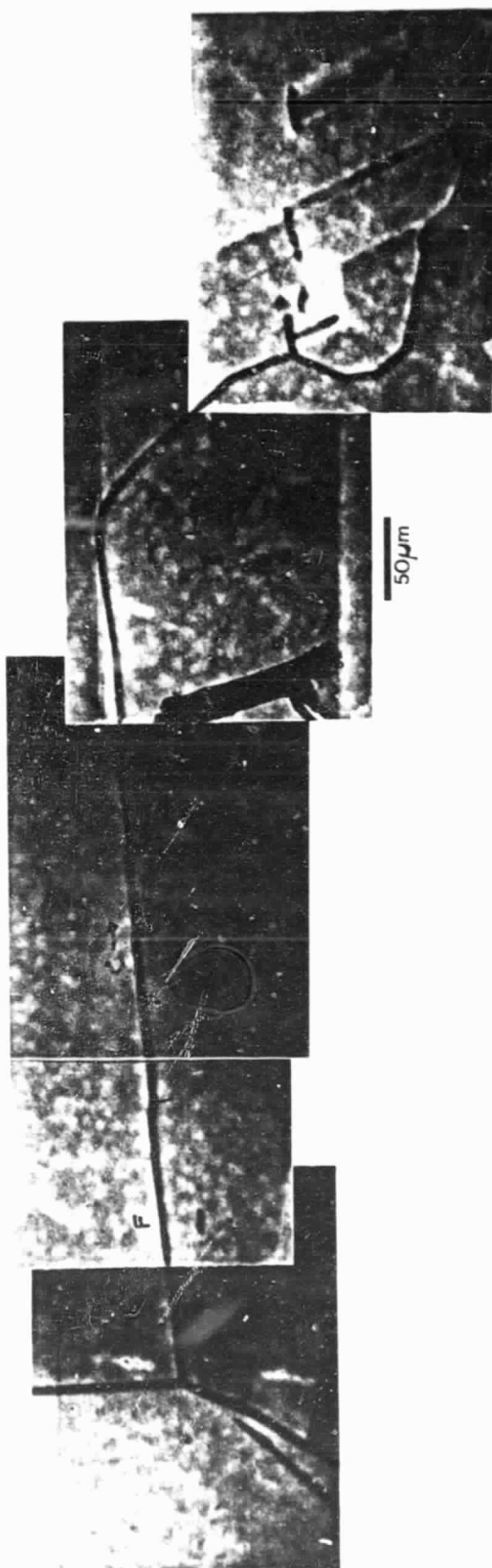
100 $\mu$ m  
(b)



50 $\mu$ m  
(c)

Figure 13

ORIGINAL PAGE  
BLACK AND WHITE PHOTOGRAPH



ORIGINAL PAGE  
BLACK AND WHITE PHOTOGRAPH

Figure 14